

# An accurate and versatile lattice closure scheme for lattice Boltzmann equation fluids under external forces

A.P. Hollis\*, I. Halliday, C.M. Care

*Materials Research Institute, Sheffield Hallam University, City Campus, Howard Street, Sheffield, South Yorkshire S1 1WB, UK*

Received 5 February 2007; received in revised form 21 January 2008; accepted 14 May 2008

Available online 24 May 2008

---

## Abstract

We derive and demonstrate a practical, analytic, versatile and accurate algorithm designed to impose Dirichlet boundary conditions (specified boundary velocity) on the edge nodes of a lattice Boltzmann fluid simulation space, valid for situations in which the fluid at the boundary is subject to a force. The current algorithm models the lattice fluid on boundary and bulk nodes to the same accuracy and in a demonstrably equivalent manner. Whilst the new method presented here applies to rectangular geometries, it adds to our previous method [I. Halliday, L.A. Hammond, C.M. Care, A. Stevens, *J. Phys. A: Math. Gen.* 35 (2002) 157]: (i) the condition of mass-conservation, (ii) the ability to subject boundary fluid to a force and (iii) the ability to treat a range of complicated geometries with unimpaired accuracy.

© 2008 Elsevier Inc. All rights reserved.

*Keywords:* Lattice Boltzmann; Simulation lattice closure

---

## 1. Introduction

Lattice Boltzmann (LB) flow simulation is adapted to certain niches; canonically, time-dependant, complex, multi-component and particle-laden flows [1]. As with any numerical method, representation of boundary conditions is central.

This article is an update of our attempts to develop a comprehensive, robust, accurate and adaptable lattice closure, able to impose boundary conditions on a LB fluid simulation. What we report here (in a self-contained manner, note) extends previous work [2,3] to facilitate (i) Navier-type boundary conditions and (ii) fluids under external forces, such as are applied to produce fluid–fluid interfaces; the essentials of multi-component LB boundary conditions for e.g. wetting. Like previous work, our current method is designed to give boundary fluid in transient flow near the boundary the same dynamics and accuracy of representation as the bulk lattice fluid (at all times), it applies transparently to complex boundary geometries (corners) with no diminution of accuracy and it admits of the representation of moving fluid boundaries, including those crossed by fluid.

---

\* Corresponding author. Tel.: +44 114 225 3068; fax: +44 114 225 3501.

*E-mail address:* [Adam.Hollis@student.shu.ac.uk](mailto:Adam.Hollis@student.shu.ac.uk) (A.P. Hollis).

Lattice closure methods in LB [1] fall into two sets. One provides Lees–Edwards type boundary conditions [4], typically for calculation of colloidal phase properties and phase separation kinematics [5,7]. The present method belongs to a second class of LB boundary closure, designed to impose a specified velocity distribution (possibly corresponding to a slip) on the defined surfaces which comprise the boundary.

In general, solutions of the Navier–Stokes and continuity equations,  $(\mathbf{v}(\mathbf{r}, t), P(\mathbf{r}, t))$ , may be closed by Dirichlet boundary conditions on fluid velocity:

$$\mathbf{v}(\mathbf{r}', t) = \mathbf{u}_0(\mathbf{r}', t). \quad (1)$$

Here  $\mathbf{r}'$  denotes a position on the flow domain boundary and  $\mathbf{u}_0(\mathbf{r}', t)$  a known boundary fluid velocity distribution. Fluid is said to stick; to have ‘no-slip’ against solid surfaces; then  $\mathbf{u}_0(\mathbf{r}', t)$  corresponds to the velocity of any solid boundaries. However, there have been doubts about the no-slip condition for more than a century [8]. Indeed, fluid close to a dynamic contact line *must* slip. One theory relates the boundary–tangent component fluid in the DCL, the slip velocity,  $v_s$ , to the tangential component of fluid shear at the surface:

$$v_s(\mathbf{r}', t) = b \left[ \frac{\partial v_t}{\partial x_n} \right]_{\mathbf{r}'t}, \quad (2)$$

in which the constant  $b$  is the *slip length*.

There are several implementations of the rest boundary condition in LB [9–17]. It is not our purpose to investigate the origin or applicability of these; rather, we aim to design a tractable, practical and versatile LB lattice closure step for a known boundary velocity (which may, like that in Eq. (2), derive from some model of slip), local mass conservation and a known boundary external force distribution.

Our method is chosen to be node-based, in contrast to robust (but less tractable) mid-link bounce-back conditions. Whilst the location of the boundary in our method must be known *a priori*, that boundary could (for a complex shape, say) be assumed to lie at any distance from a node.

After reviewing salient theory in Section 2, we consider a flat boundary at which fluid is moving with specified velocity, subject to a specified, external body force, in Section 3.1. We summarize equivalent results for internal and external corners in Section 3.2. To evaluate our method, Section 4 presents accuracy plots, profiles of solved, pressure driven duct flows with moving and stationary boundaries and stream functions.

Only at certain stages in our analysis will it be necessary to use a particular LB model. At such points we will use a 2D, nine velocity D2Q9 single relaxation time LBGK model of Qian and d’Humières [18], as derived by Hou et al. [19].

## 2. Background

Collision and propagation of LBs momentum density function,  $f_i(\mathbf{r}, t)$ ,  $i = 0 \dots 8$ , may be expressed [1]:

$$f_i(\mathbf{r} + \mathbf{c}_i \delta_t, t + \delta_t) \equiv f_i^\dagger(\mathbf{r}, t) = f_i(\mathbf{r}, t) + \Omega_{ij} \left( f_j^{(0)}(\rho, \mathbf{v}) - f_j(\mathbf{r}, t) \right) + \phi_i, \quad (3)$$

where  $\delta_t$  represents the time step,  $f_i^\dagger(\mathbf{r}, t)$  the post-collision, pre-propagate value of the momentum density and  $\Omega_{ij}$  the collision matrix [1]. For link vectors,  $\mathbf{c}_i$ , and indexing of the velocity basis  $\mathbf{c}_i$ , see Fig. 1. The term  $\phi_i$  in Eq. (3) is responsible for introducing an external force on the fluid and is further discussed at the end of this section. Until further notice, suppose that  $\phi_i = \text{constant}$  everywhere, corresponding to uniform external force on the fluid.

In general, in  $D$  dimensions, the lattice fluid’s kinematic viscosity is determined by the degenerate eigenvalue,  $\Lambda$ , of the circulant, symmetric collision matrix  $\Omega_{ij} = \Omega_{ji}$  with the  $\frac{1}{2}D(D+1)$  *stress mode* eigenvectors  $|c_{i\alpha}c_{i\beta}\rangle$ . For the single relaxation time LBGK model [18],  $\Omega_{ij}$  and  $\Lambda$  are:

$$\Omega_{ij} = \frac{1}{\tau} \delta_{ij}, \quad \Lambda = \frac{1}{\tau}, \quad (4)$$

and, for our particular D2Q9 LBGK model the fluid’s kinematic viscosity is [19]:

$$\nu = \left( \frac{2\tau - 1}{6} \right) \frac{\delta x^2}{\delta_t}. \quad (5)$$

Note that the lattice spacing  $\delta x = 1$  throughout and that the  $\Omega_{ij}$  or  $\tau$  are assumed to be known.

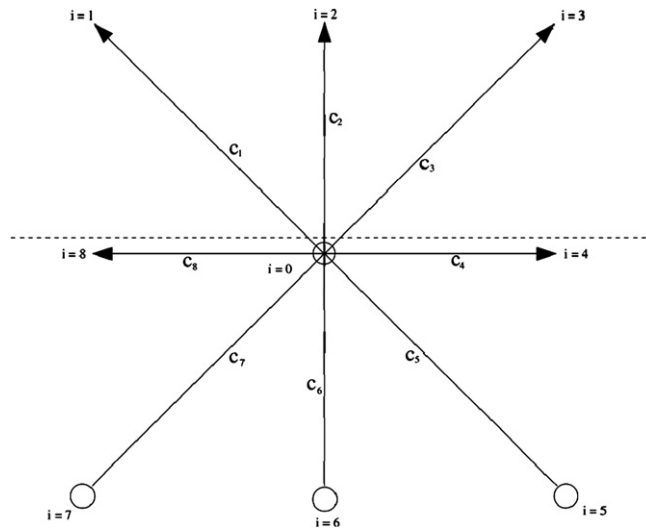


Fig. 1. A boundary node on a horizontal wall, immediately prior to a collision step. Links  $i = 1, 2, 3$  all point into solid boundary, *live* links  $i = 0, 4 \dots 8$  all point into fluid. The supposed rest wall location is denoted by the horizontal dashed line.  $f_i$ s exist for links depicted with an arrowhead, lack of  $f_i$ s is denoted by an open circle.

The macroscopic fluid density and momentum, obtained from moments of the  $f_i$ s:

$$\begin{aligned} \rho &= \sum_i f_i, \\ \rho \mathbf{v} &= \sum_i f_i \mathbf{c}_i, \end{aligned} \tag{6}$$

alone determine the principal contribution to  $f_i$ , the so-called equilibrium distribution function,  $f_i^{(0)}$  (other, smaller, contributions to  $f_i$  are discussed around Eq. (12), shortly). For all LB models  $f_i^{(0)}$  is linear in  $\rho$ :

$$f_i^{(0)}(\rho, \mathbf{v}) = \rho P^{(2)}(\mathbf{v} \cdot \mathbf{c}_i), \tag{7}$$

where the second-order polynomial  $P^{(2)}(\mathbf{v} \cdot \mathbf{c}_i)$  depends upon the particular LB model. For the LBGK model:

$$f_i^{(0)}(\rho, \mathbf{v}) = t_p \rho \left[ 1 + \frac{\mathbf{v} \cdot \mathbf{c}_i}{c_s^2} - \frac{v^2}{2c_s^2} + \frac{(\mathbf{v} \cdot \mathbf{c}_i)^2}{2c_s^4} \right], \tag{8}$$

where  $t_p = 4/9, 1/9, 1/36$  for  $i = 0, i$  even,  $i$  odd respectively and the speed of sound  $c_s = 1/\sqrt{3}$  [19,18]. The  $f_i^{(0)}$  provide the principal contribution to  $f_i$  and have the following moments with the lattice links  $\mathbf{c}_i$ :

$$\begin{aligned} \rho &= \sum_i f_i^{(0)}, \\ \rho \mathbf{v} &= \sum_i f_i^{(0)} \mathbf{c}_i, \end{aligned} \tag{9}$$

$$\Pi_{\alpha\beta}^{(0)} \equiv c_s^2 \rho \delta_{\alpha\beta} + \rho v_\alpha v_\beta = \sum_i f_i^{(0)} c_{i\alpha} c_{i\beta}, \tag{10}$$

$$c_s^2 \rho (u_\gamma \delta_{\alpha\beta} + u_\alpha \delta_{\beta\gamma} + u_\beta \delta_{\alpha\gamma}) = \sum_i f_i^{(0)} c_{i\alpha} c_{i\beta} c_{i\gamma}, \tag{11}$$

in which Eq. (10) defines a momentum flux tensor. The squared speed of sound,  $c_s^2 = 1/3$  and lattice symmetry constant  $k_4 = 1/9$  in the LBGK D2Q9 model.

The effects on the lattice fluid of higher order contributions to  $f_i$ , denoted  $f_i^{(n>0)}$ , are understood through the Chapman–Enskog expansion method [1]. Taking the particular Chapman–Enskog approach of Hou et al. [19] write:

$$f_i = f_i^{(0)} + \delta_t f_i^{(1)} + \cdots + \delta_t^n f_i^{(n)} + \cdots, \quad (12)$$

from which Navier–Stokes behaviour (with a uniform body force acting) may be recovered with  $n < 2$  [19] (note in passing that, for consistency, a boundary node momentum density,  $f_i$ , should therefore be correct to  $f_i^{(1)}$ ). Derivation, by Chapman–Enskog analysis, of such Navier–Stokes behaviour only trivially affected by the presence in our evolution Eq. (3) of the term  $\phi_i$  if the latter is has zero derivatives. However, when  $\phi_i$  varies it is necessary to modify the definitions (9) and perform a more careful Chapman–Enskog analysis in order to obtain Navier–Stokes behaviour at the same level of accuracy [20]. We return to this issue below. For the moment, Eq. (9) ensures that zeroth and first moments of  $f_i^{(1)}$  are zero:

$$\sum_i f_i^{(n>0)} \Delta_i = 0, \quad n > 0, \quad (13)$$

where  $\Delta_i = 1, c_{ix}, c_{iy}$  but the second moments of the the  $f_i^{(1)}$  are not zero. Using a Chapman–Enskog method directly adapted from that of Hou et al. [19], it is straightforward to show that the latter provide a local expression for the lattice fluid rate of strain:

$$\left(\frac{\Lambda}{2} - 1\right) \sum_i f_i^{(1)} c_{ix} c_{i\beta} = 2\nu\rho S_{\alpha\beta}, \quad (14)$$

where  $S_{\alpha\beta} = 1/2(\partial_\alpha v_\beta + \partial_\beta v_\alpha)$  and, recall,  $\Lambda = \frac{1}{\tau}$  for an LBGK model. It is convenient to re-express Eq. (14):

$$\sum_i f_i^{(1)} c c_{i\alpha\beta} = 2\nu\rho S_{\alpha\beta}, \quad c c_{i\alpha\beta} \equiv \left(\frac{\Lambda}{2} - 1\right) c_{ix} c_{i\beta}. \quad (15)$$

In  $D$  dimensions, Eq. (15) number  $D(D+1)/2$ ; Eq. (13) number  $(D+1)$ . In total Eqs. (15) and (13) provide  $(D+1)(D/2+1)$  equations for  $Q$   $f_i^{(1)}$ s. Therefore, in the case of a D2Q9 LBGK model, Eqs. (13) and (15) yield a total of six equations for  $Q=9$ ,  $f_i^{(1)}$ s. Also for a D2Q9 LBGK model, Eqs. (4) and (5) may be used to simplify Eq. (15):

$$\sum_i f_i^{(1)} c_{ix} c_{i\beta} = -2c_s^2 \rho \tau S_{\alpha\beta}. \quad (16)$$

Using Eqs. (3) and (12) (with  $n < 2$ ), it is possible to express the collision part of the evolution as a relaxation of (just) the  $f_i^{(1)}$  component of  $f_i(\mathbf{r}, t)$ :

$$f_i^\dagger(\mathbf{r}, t) = f_i^{(0)}(\rho, \mathbf{v}) + \left[ f_i^{(1)\dagger} \equiv \delta_t \sum_i (\delta_{ij} - \Omega_{ij}) f_j^{(1)} \right] + \phi_i + o\left(\delta_t^2 f_i^{(2)}\right), \quad (17)$$

that is collision may be represented by a replacement:

$$f_i^{(1)} \rightarrow f_i^{(1)\dagger}, \quad f_i^{(1)\dagger} = \sum_i (\delta_{ij} - \Omega_{ij}) f_j^{(1)}, \quad (18)$$

and the addition of source term,  $\phi_i$ ; note that we have set  $\delta_t = 1$  here. In the current context, using Eqs. (4), (18) simplifies to make LBGK an attractive option:

$$f_i^{(1)\dagger} = \left(1 - \frac{1}{\tau}\right) f_i^{(1)}. \quad (19)$$

Let us now consider the term  $\phi_i$  in Eqs. (3) and (17).  $\phi_i$  is a source term used, so far, to impress a uniform external force on the lattice fluid at the Navier–Stokes level, say to represent a uniform pressure gradient,  $\mathbf{g}$ . For simplicity, we have neglected spatial variation in the macroscopic force, taking the macroscopic momentum equation arising from Eq. (3) to be:

$$\frac{\partial}{\partial t} \rho v_\alpha + \frac{\partial}{\partial x_\beta} \rho v_\beta v_\alpha = -\frac{\partial}{\partial x_\alpha} \rho + \frac{\partial}{\partial x_\beta} (2\rho\nu S_{\alpha\beta}) + \left[ g_\alpha \equiv \sum_i \phi_i c_{ix} \right], \quad (20)$$

in which all other symbols and notations have their usual meaning. We note in passing that forcing a fluid in the bulk of the simulation lattice must conserve nodal density, hence:

$$\sum_{i=0}^{(Q-1)} \phi_i = 0, \tag{21}$$

but, since a force is acting,  $\sum_{i=0}^{(Q-1)} \phi_i \mathbf{c}_i \neq \mathbf{0}$ .

Now, the relationship between the  $\phi_i$ s and a *variable* macroscopic force has been considered by Ladd and Verberg [21] and by Guo et al. [20]. One instance of the use of a variable body force arises in applying interfacial tension in LB models. All multi-component lattice Boltzmann fluids have interfaces produced by phase index coupled pressure tensor fluctuations within what is a single effective fluid [1]. These fluctuations can be considered as (segregating) external forces of variable direction and magnitude, impressed in certain regions of a single fluid. Such interface forcing is represented by an appropriate choice of source term  $\phi_i$  in Eq. (3) and, in bulk simulations or with periodic boundaries, mass (but not momentum) is conserved. Following Ladd and Verberg [21], Guo et al. [20] show that to recover Navier–Stokes behaviour in a lattice fluid subject to a variable external force,  $\mathbf{g}(\mathbf{r})$ , it is necessary to re-define the lattice fluid velocity of Eq. (9):

$$\rho \mathbf{v} = \sum_i f_i \mathbf{c}_i + \frac{1}{2} \mathbf{g}, \tag{22}$$

and (as we show in Appendix 1, using the analysis of Guo et al.) to re-interpret the fluid strain rate,  $S_{\alpha\beta}$ .

Consider LB fluid under a constant external force. Boundary and bulk fluid should be under the same external force. We assume this force is known; the problem we seek to address is that the corresponding source term does not conserve mass on that subset of lattice links which are not cut by the boundary (see Fig. 1, in which links indexed  $i = 1, 2, 3$  are cut by a horizontal boundary). Put more precisely, partial totals of a source term are not necessarily zero:

$$\sum'_i \phi_i \neq 0, \tag{23}$$

where the symbol  $\sum'_i$  indicates a summation over a restricted range of subscript  $i$ , which excludes the value(s) of  $i$  corresponding to cut link(s).

In our analysis below that an effective fluid velocity (which may correspond to a pre-calculated slip from a chosen model eg Eq. (2), note) and external force must always be known on the boundary. For simplicity we shall assume, in the main part of this article, that the fluid is under a constant external force, like gravity. The adjustments necessary to incorporate variable external forces into our analysis are detailed in Appendix 1.

### 3. Lattice closure algorithm for forced boundary fluid

Mass conservation is a widely used assumption when closing LB simulations with Dirichlet boundary conditions. This assumption becomes unavoidable when multiple fluids are in contact at a solid boundary. We aim here to calculate momentum densities,  $f_i$ , for links of a boundary node which (i) evolve according to rules equivalent to those governing bulk nodes, (ii) are consistent with a known, local, boundary velocity (including a slip velocity), (iii) are consistent with a known constant external force and (iv) will conserve mass locally.

#### 3.1. Planar boundary

For definiteness, consider the planar boundary site on the LBGK D2Q9 lattice shown in Fig. 1. The dotted line indicates the uppermost extent of the lattice fluid. Links  $i = 1, 2, 3$  are cut. At the end of a propagation step, a *pre-collision* value of  $f_i$ , exists for all *incoming* links  $i \neq 5, 6, 7$ ; a situation represented by use of empty circles. It is necessary impress an external force on the boundary fluid; that is, to use a source term  $\phi_i$  in Eq. (3). Say that the node of Fig. 1 bounds a flow driven by a uniform, external body force in the  $x$ -direction, representing gravity, this force is obtained from a source term  $\phi_i = t_p G c_{ix}$ , where  $G = \frac{g}{c_s^2}$ .

Relative to Fig. 1, denote as *live* those links which require post-collision values of  $f_i^+$ ; links  $i \neq 1, 2, 3$  in Fig. 1 are live, for they connect into the flow domain.  $f_i$ s on *dead* links propagate into the boundary. For

the geometry of Fig. 1, pre-collision  $f_i$ s exist on *incoming* links  $i = 0, 1, 2, 3, 4, 8$ ; post-collision  $f_i^\dagger$ s are required only for live links  $i = 0, 4, 5, 6, 7, 8$ .

Boundary mass conservation is defined by equality between partial sums of the  $f_i$ s and (different) partial sums of the  $f_i^\dagger$ s. For the geometry of Fig. 1, mass conservation is

$$\left( M \equiv \sum_{i \neq 5,6,7} f_i \right) = \sum_{i \neq 1,2,3} f_i^\dagger. \tag{24}$$

Applying a force on boundary nodes does not conserve mass on live links. Again for the geometry of Fig. 1, a mass:

$$\delta M = \sum_{i \neq 1,2,3} \phi_i \tag{25}$$

is introduced into the flow domain by the macroscopic force.

We think of nodes as being evolved by collision and propagation, with collisions described by Eq. (17). We construct post-collision, boundary  $f_i$ s, instantaneously correct to the accuracy of the bulk LB model in 4 steps:

1. Determine  $M$  ( $\delta M$ ) from an appropriate form of Eq. (24) ((25)):

$$M = \sum_{\text{incoming}} f_i, \tag{26}$$

$$\delta M = \sum_{\text{live}} \phi_i. \tag{27}$$

2. Determine the  $f_i^{(0)}(\rho', \mathbf{u}_0)$ s from *effective* density,  $\rho'$ :

$$\sum_{\text{live}} f_i^{(0)}(\rho', \mathbf{u}_0) = M - \delta M, \tag{28}$$

summation being taken over *is* corresponding to live links:  $M$ , ( $\delta M$ ) being defined in Eq. (26), ((27)).

3. Determine pre-collision  $f_i^{(1)}$ s from an under-specified system after Eqs. (13) and (16).
4. Collide the boundary sites using Eq. (17).

A few remarks before detailing steps 1 . . . 4 above. We note that the condition of boundary mass conservation is satisfied only after the completion of final step (4). Also, the under-specified system solved for the  $f_i^{(1)}$ s in step (3) is an adaptation of  $(D + 1)(D/2 + 1)$  Eqs. (13) and (16), namely:

$$\sum_{\text{live}} f_i^{(1)} = 0, \tag{29}$$

$$\sum_i f_i^{(1)} c_{iz} = 0, \tag{30}$$

$$\sum_i f_i^{(1)} c c_{iz\beta} = 2\rho' v S_{z\beta}, \tag{31}$$

where, note, the range of  $i$ -summation in Eq. (29) only is restricted, whilst that in Eqs. (30) and (31) is not. This maintains consistency correspondence with the bulk algorithm whilst ensuring that the  $f_i^{(1)}$ s have zero contribution to the total mass on live links.

In the above system of Eqs. (29) and (30) are independent of particular LB model, however the  $D(D + 1)/2$  Eq. (31) depend upon model through the  $\Omega_{ij}$  (see Eq. (15)). Finally we note that the corresponding, post-collision, values  $f_i^{(1)\dagger}$  are a simple linear combination of the solution of Eqs. (29)–(31) above (see Eq. (18)).

*Step 1:* Evaluate  $M$  and  $\delta M$  using the definitions in Eqs. (24) and (25) respectively.

*Step 2:* The boundary (or slip) velocity  $\mathbf{u}_0$  is known. Eqs. (7) and (28) provide an identity for effective boundary node density,  $\rho'$ :

$$\rho' = \frac{M - \delta M}{\sum_{\text{live}} P^{(0)}(\mathbf{u}_0 \cdot \mathbf{c}_i)}. \tag{32}$$

For the example geometry of Fig. 1 and the corresponding LBGK equilibrium, Eq. (32) is

$$\rho' = \frac{M - \delta M}{\sum_{i \neq 1,2,3} t_p \left[ 1 + \frac{\mathbf{u}_0 \cdot \mathbf{c}_i}{c_s^2} - \frac{u_0^2}{2c_s^2} + \frac{(\mathbf{u}_0 \cdot \mathbf{c}_i)^2}{2c_s^4} \right]} = \frac{6(M - \delta M)}{5 + 3u_{0y} - 3u_{0y}^2}, \tag{33}$$

in which, note, velocity component  $u_{0x}$  does not appear. To evaluate  $\delta M$  from Eq. (27) (or Eq. (25)) requires the values of live source terms,  $\phi_i$ . For our chosen example (a uniform body force in the  $x$ -direction, recall  $\phi_i = t_p G c_{ix}$ :

$$\delta M = G \sum_{i \neq 1,2,3} t_p c_{ix}. \tag{34}$$

It is now possible to assign  $\rho'$  from Eq. (33) and hence obtain  $f_i^{(0)}(\rho', \mathbf{u}_0)$ .

*Step 3:* For our chosen example boundary, flow and model equations (29)–(31) yield:

$$\sum_{i \neq 1,2,3} f_i^{(1)} = 0, \tag{35}$$

$$\sum_i f_i^{(1)} c_{i\alpha} = 0, \quad \alpha = x, y, \tag{36}$$

$$\sum_i f_i^{(1)} c_{i\alpha} c_{i\beta} = -\frac{2}{3} \rho' \tau S_{\alpha\beta}, \quad \alpha = x, y, \beta = x, y, \tag{37}$$

in the last of which we have used Eqs. (15) and (4). Here then, nine  $f_i^{(1)}$ ,  $i = 0 \dots 8$  satisfy the six Eqs. (35)–(37) re-formatted below:

$$\begin{aligned} f_0^{(1)} + 0f_1^{(1)} + 0f_2^{(1)} + 0f_3^{(1)} + f_4^{(1)} + f_5^{(1)} + f_6^{(1)} + f_7^{(1)} + f_8^{(1)} &= 0, \\ f_0^{(1)} + f_4^{(1)} + f_5^{(1)} + f_6^{(1)} + f_7^{(1)} + f_8^{(1)} &= 0, \\ -f_1^{(1)} + f_3^{(1)} + f_4^{(1)} + f_5^{(1)} - f_7^{(1)} - f_8^{(1)} &= 0, \\ f_1^{(1)} + f_2^{(1)} + f_3^{(1)} - f_5^{(1)} - f_6^{(1)} - f_7^{(1)} &= 0, \\ f_1^{(1)} + f_3^{(1)} + f_4^{(1)} + f_5^{(1)} + f_7^{(1)} + f_8^{(1)} &= -2\rho\tau/3S_{xx}, \\ f_1^{(1)} + f_2^{(1)} + f_3^{(1)} + f_5^{(1)} + f_6^{(1)} + f_7^{(1)} &= -2\rho\tau/3S_{yy}, \\ -f_1^{(1)} + f_3^{(1)} - f_5^{(1)} + f_7^{(1)} &= -2\rho\tau/3S_{xy}. \end{aligned} \tag{38}$$

The absence of  $f_1^{(1)}$ ,  $f_2^{(2)}$  and  $f_3^{(3)}$  from the first of Eq. (38) (which derives from Eq. (35)) has been emphasized. Note, the surface strain rates in the right hand side of last three equations must all be determined, in our case using spatially  $o(3)$  accurate finite-differences. Note that in the case of slip, these finite difference expressions, which involve the instantaneous surface slip velocity, were assumed simply to assign a quasi-statically developing slip velocity at the next time.

When applying our LB method to other models, differences must be assumed to arise at this point. For a 3D LBGK model, a system similar to Eq. (14) results; for general LB models the system of equations corresponding to Eq. (38) would contain coefficients of the  $f_i^{(1)}$ s which are linear combinations of the  $\Omega_{ijs}$  (see e.g. Eq. (14)).

To solve the under-determined system of Eq. (38), select a triplet of known  $f_i^{(1)}$ s as free variables. Certain triplets of the free  $f_i^{(1)}$ s are forbidden, which may be understood as follows. Defining quantities:

$$\begin{aligned} g_1 &\equiv f_1^{(1)} + f_2^{(1)} + f_3^{(1)}, \\ g_2 &\equiv f_5^{(1)} + f_6^{(1)} + f_7^{(1)}, \\ g_3 &\equiv f_3^{(1)} + f_4^{(1)} + f_5^{(1)}, \\ g_4 &\equiv f_1^{(1)} + f_7^{(1)} + f_8^{(1)}, \\ g_5 &\equiv f_0^{(1)} + f_4^{(1)} + f_8^{(1)}, \end{aligned} \tag{39}$$

the first five of the six Eq. (38) may be written:

$$\begin{aligned}
 g_2 + g_5 &= 0, \\
 g_3 - g_4 &= 0, \\
 g_1 - g_2 &= 0, \\
 g_3 + g_4 &= -2\rho\tau/3S_{xx}, \\
 g_1 + g_2 &= -2\rho\tau/3S_{yy}
 \end{aligned}
 \tag{40}$$

which system (40) may be solved for the  $g_1, \dots, g_5$  in terms of the  $S_{\alpha\beta}$ . The value of (say)  $g_1$  so obtained constrains the sum  $f_1^{(1)} + f_2^{(1)} + f_3^{(1)}$ ; accordingly  $f_1^{(1)}, f_2^{(1)}$  and  $f_3^{(1)}$  cannot all be assigned; cannot all be free variables. Forbidden triplets of free  $f_i^{(1)}$ s for our example system are defined in Table 1, alongside a diagrammatic interpretation. Note, the sixth equation in the system 38 cannot be expressed in terms of  $g_1 \dots g_5$ .

Above we referred to *known*  $f_i^{(1)}$ s. In addition to the structure of system (40), the set of three  $f_i^{(1)}$ s selected as free variables should depend upon which links,  $\mathbf{c}_i$ , contain information originating from within the flow domain. To solve Eqs. (35)–(37) then, we use free variable  $f_i^{(1)}$ s which (i) do not comprise a forbidden set and (ii) have accessible values.

We choose as free variables in the solution of Eqs. (35)–(37):

$$f_i^{(1)} \approx \left( f_i - f_i^{(0)}(\rho t, \mathbf{u}_0) \right), \quad i = 0, 1, 2,
 \tag{41}$$

in terms of which the solution (of system of Eqs. (38)) is

$$\begin{aligned}
 f_3^{(1)} &= -\kappa S_{yy} - f_1^{(1)} - f_2^{(1)}, \\
 f_4^{(1)} &= \frac{3}{2}\kappa S_{yy} - \kappa S_{xy} - \frac{1}{2}f_0^{(1)} + 2f_1^{(1)} + f_2^{(1)}, \\
 f_5^{(1)} &= -\kappa S_{xx} - \frac{1}{2}\kappa S_{yy} + \kappa S_{xy} + \frac{1}{2}f_0^{(1)} - f_1^{(1)}, \\
 f_6^{(1)} &= 2\kappa S_{xx} - \kappa S_{yy} - f_0^{(1)} - f_2^{(1)}, \\
 f_7^{(1)} &= -\kappa S_{xx} + \frac{1}{2}\kappa S_{yy} - \kappa S_{xy} + \frac{1}{2}f_0^{(1)} + f_1^{(1)} + f_2^{(1)}, \\
 f_8^{(1)} &= -\frac{1}{2}\kappa S_{yy} - \kappa S_{xy} - \frac{1}{2}f_0^{(1)} - 2f_1^{(1)} - f_2^{(1)},
 \end{aligned}
 \tag{42}$$

where

$$\kappa \equiv c_s^2 \rho \tau.
 \tag{43}$$

Our choice of free variables  $f_i^{(1)}$ ,  $i = 0, 1, 2$  is not unique. We shall return to this point in Section 4.

Table 1

Diagrammatic representation of the forbidden triplet combinations of  $f_i^{(1)}$ s as free variables for the planar boundary geometry of Fig. 1

Forbidden set of three free $f_i^{(1)}$ s	Link representation
$f_1^{(1)}, f_2^{(1)}, f_3^{(1)}$	
$f_3^{(1)}, f_4^{(1)}, f_5^{(1)}$	
$f_5^{(1)}, f_6^{(1)}, f_7^{(1)}$	
$f_1^{(1)}, f_7^{(1)}, f_8^{(1)}$	
$f_0^{(1)}, f_4^{(1)}, f_8^{(1)}$	

The small (large) dot represents inclusion (exclusion) of the rest link.



Step 4: The pre-collision boundary node  $f_i^{(1)}$ 's constructed in step 2 are collided, using Eq. (17), then added to the corresponding  $f_i^{(0)}(\rho', \mathbf{u}_0)$ , yielding a post-collision momentum density:

$$f_i^\dagger(\mathbf{r}, t) = f_i^{(0)}(\rho', \mathbf{u}_0) + \sum_i (\delta_{ij} - \Omega_{ij}) f_j^{(1)} + \phi_i, \tag{44}$$

which, for the example LBGK system, reduces to:

$$f_i^\dagger(\mathbf{r}, t) = f_i^{(0)}(\rho', \mathbf{u}_0) + \left(1 - \frac{1}{\tau}\right) f_i^{(1)} + \phi_i, \tag{45}$$

Before proceeding to consider other boundary shapes (corners), a few remarks are in order. We note that the analysis of this section is valid, stability issues notwithstanding, for any value of collision parameter  $\tau$ . Of course, the choice of the free variables should not affect the accuracy or stability of the resulting closure scheme. We shall return to this issue in Section 4.

### 3.2. Application to complex geometry

We illustrate the versatility of the method outlined in Section 3.1 by treating, albeit in less detail, internal and external corners. Consider our example D2Q9 LBGK system system.

**Internal corner.** Fig. 2 shows a top left internal corner boundary node. The dotted line shows the supposed location of the boundary. Quantities  $f_3, f_7$  (links represented by broken lines) are *ghost* (not, note, dead) quantities which never participate.  $f_0^\dagger, f_4^\dagger, f_5^\dagger$  and  $f_6^\dagger$  are required. For the geometry of Fig. 2 the appropriate value of  $M$  is

$$M \equiv \sum_{i \neq 3,4,5,6,7} f_i, \tag{46}$$

and the value of  $\rho'$  is therefore given by

$$\rho' = \frac{M - \delta M}{\sum_{i \neq 1,2,3,7,8} t_p \left[ 1 + \frac{\mathbf{u}_0 \cdot \mathbf{c}_i}{c_s^2} - \frac{u_0^2}{2c_s^2} + \frac{(\mathbf{u}_0 \cdot \mathbf{c}_i)^2}{2c_s^4} \right]}, \tag{47}$$

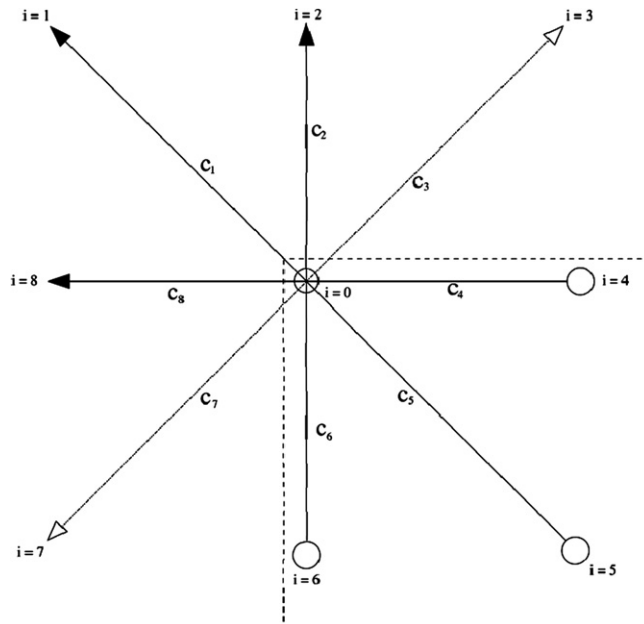


Fig. 2. A boundary node on a ‘top left’ internal corner, immediately prior to a collision step. The supposed locations of the rest walls are denoted by the dashed lines. Links  $i = 0, 5, 6, 6$  are live. Note, the  $i = 0$  link lies in the fluid.  $f_i$ s exist (do not exist) for links depicted with an arrowhead (open circle). Ghost links, which never participate, are indicated by open arrowheads.

where  $\delta M$  is the mass associated with the source terms to be added on the live links (see Eq. (25)):

$$\delta M \equiv \sum_{i \neq 1,2,3,7,8} \phi_i. \tag{48}$$

With some straightforward algebra:

$$\rho' = \frac{36(M - \delta M)}{25 + 15u_{0x} - 15u_{0y} - 9u_{0x}u_{0y} - 15u_{0x}^2 - 15u_{0y}^2}. \tag{49}$$

The condition corresponding to Eq. (35) for this geometry is

$$\sum_{i \neq 1,2,3,7,8} f_i^{(1)} = 0. \tag{50}$$

Solving for pre-collision  $f_i^{(1)}$ s follows the procedure in Section 3.1. No forbidden triplets of obtainable  $f_i^{(1)}$ s arise for the case of 2D, D2Q9 internal corner geometry.

**External corner.** Fig. 3 shows an external corner. The dotted line shows the supposed location of the boundary.  $f_0^\dagger, f_1^\dagger, f_2^\dagger, f_3^\dagger, f_4^\dagger, f_6^\dagger, f_7^\dagger$  and  $f_8^\dagger$  are required. For  $M, \delta M$  and  $\rho'$  we now have:

$$M = \sum_{i \neq 1} f_i, \tag{51}$$

and:

$$\delta M = \sum_{i \neq 5} \phi_i. \tag{52}$$

and (after some algebra):

$$\rho' = \frac{36(M - \delta M)}{35 - 3u_{0x} - 3u_{0y} + 3u_{0x}^2 + 9u_{0x}u_{0y} - 3u_{0y}^2}. \tag{53}$$

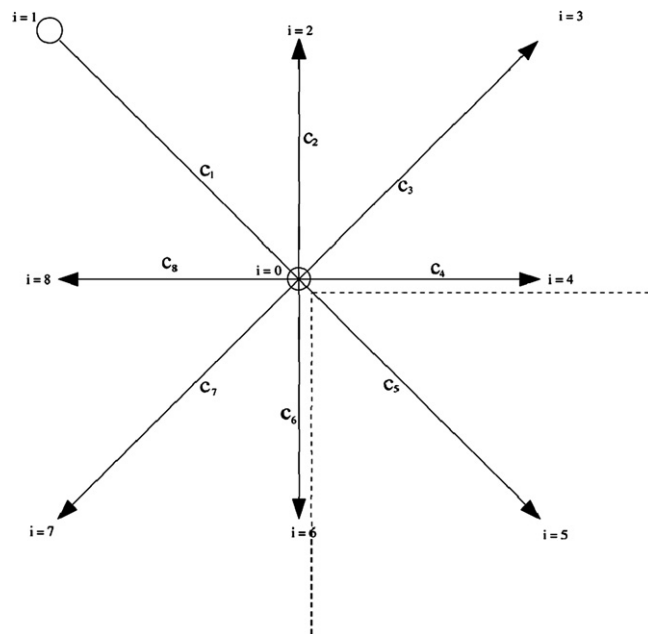




Fig. 3. A boundary node on an external corner. The rest walls' locations are denoted by the dashed lines; the  $i = 0$  link lies in the fluid.  $f_i$ s exist (do not exist) for links depicted with an arrowhead (open circle).

Table 2

Diagrammatic representation of the forbidden triplet combinations of  $f_i^{(1)}$ s as free variables, for the external corner geometry of Fig. 3

Forbidden set of three free $f_i^{(1)}$ s	Link representation
$f_0^{(1)}, f_6^{(1)}, f_7^{(1)}$	
$f_0^{(1)}, f_4^{(1)}, f_3^{(1)}$	

Note that the large dot indicates that the rest link is included. Unlike Table 1, only triplet combinations which contain three  $f_i^{(1)}$ s all of which may be evaluated in practice are listed here.

The mass conservation condition corresponding to Eq. (35) for this geometry is

$$\sum_{i \neq 5} f_i^{(1)} = 0. \tag{54}$$

Solving for pre-collision  $f_i^{(1)}$ s again follows the procedure in Section 3.1. Triplets of evaluatable  $f_i^{(1)}$ s now forbidden are listed in Table 2. Clearly other geometries and other situations are amenable to the boundary analysis of this section. Situations in 3D, corresponding to any number of cut links are a straightforward generalization of current method. Further extension to off-lattice boundaries is more complicated; it requires no fundamental modification to the method.

#### 4. Analysis and results

In order to assess our method for time-dependant boundary conditions, we considered the development of incompressible flow in a uniform channel, width  $W$ , bounded by stationary surfaces  $y = \text{constant}$  and, in the horizontal direction, by periodic boundary conditions. Flow was driven (for  $t > 0$ ) by a uniform pressure gradient  $\frac{\partial p}{\partial x} = g$  corresponding to  $\phi_i = t_p G c_{ix}$  at  $t = 0^+$  and the lattice fluid was initialized by assigning  $f_i(\mathbf{r}, 0) = f_i^{(0)}(\rho, \mathbf{0})$  everywhere. Note that  $G = 3g$  [22]. To generate additional interest the planar boundaries  $y = 0^-, W^+$  were assumed to admit slip, described by a slip velocity instantaneously in accord with Eq. (2). A range of slip lengths  $b = 0.005, 0.05, 0.5$  were used. With no-slip boundary conditions, the corresponding flow has a characteristic time [2]:

$$T_0 = \frac{\nu}{W^2}. \tag{55}$$

$v_s/V_0$ , the instantaneous slip velocity, normalized to the slip velocity measured at  $t = T_0/2$ , was obtained from a numerical solution (explicit, time-marching scheme) of the 2D, time-dependant Navier–Stokes equations, for times  $t < T_0/2$ ; this solution is, in Fig. 4, found to be in excellent agreement with values obtained from the corresponding LB simulations using our boundary closure, over the range of slip lengths.

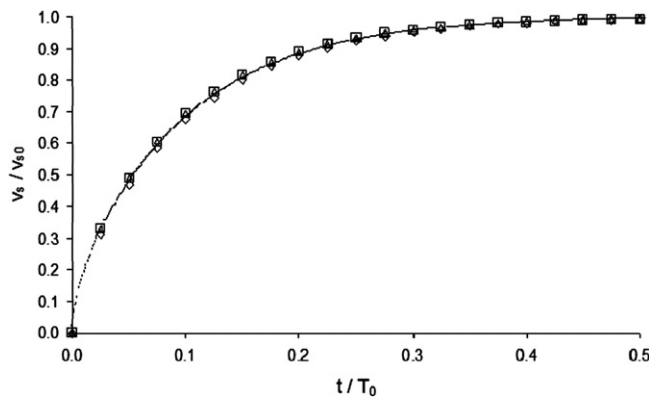


Fig. 4. Evolution of the boundary slip velocity in pressure-driven duct flow. The time normalization parameter is  $T_0 = \frac{\nu}{W^2}$ . The line shows a numerical solution, the open triangles (squares) ((diamonds)) correspond to slip length  $b = 0.005$  ( $b = 0.05$ ) ( $b = 0.5$ ).

Consider now the steady state corresponding to the flow considered above, now with no-slip, Dirichlet boundary conditions. Invoking translational invariance in the  $x$ -direction and the fact that  $\rho = \text{constant}$  everywhere, it is straightforward to obtain the steady-state solution,  $(v_0(y), 0)$ , to the lattice fluid’s Navier–Stokes equation (20):

$$v_0(y) = \frac{G}{6\rho\nu}y(W - y), \tag{56}$$

which we now proceed to use quantitatively to assess the accuracy of the solution obtained from simulations closed using the method of Section 3.1.

Flow rate and hence Reynolds’ number:

$$Re \equiv \frac{\bar{v}W}{\nu} = \frac{GW^3}{36\rho\nu^2} \tag{57}$$

was controlled by the value of  $G$  used in the source term  $\phi_i = t_p G c_{ix}$  of the LBGK adapted evolution Eq. (3). A total absolute error:

$$\Delta_W \equiv \sum_{y \neq 0} |v_m(y) - v_0(y)|, \tag{58}$$

was defined, where  $v_m(y)$  denotes the simulated, parabolic profile obtained with the boundary closure method of Section 3.1.  $v_m(y)$  was measured at constant  $Re = 0.5$  for a range of lattice widths (resolutions)  $W = 10 \times 2^N$ ,  $N \leq 5$ .

The data of Fig. 5 shows the value of  $\log_{10}(\Delta_W)$  as a function of resolution, measured by  $\log_{10}W$ . The collision parameter for this particular data was  $\tau = 2/3$ , however, use of  $\tau = 1, 2$  produce no change in the data presented in Fig. 5 visible to the eye, as discussed below.

The results in Fig. 5 comprise two almost overlying, sets of points (a) and (b). Data set (a) is comprised of open squares and diagonal crosses, data set (b) of open circles and erect crosses. Sets (a) and (b) are based

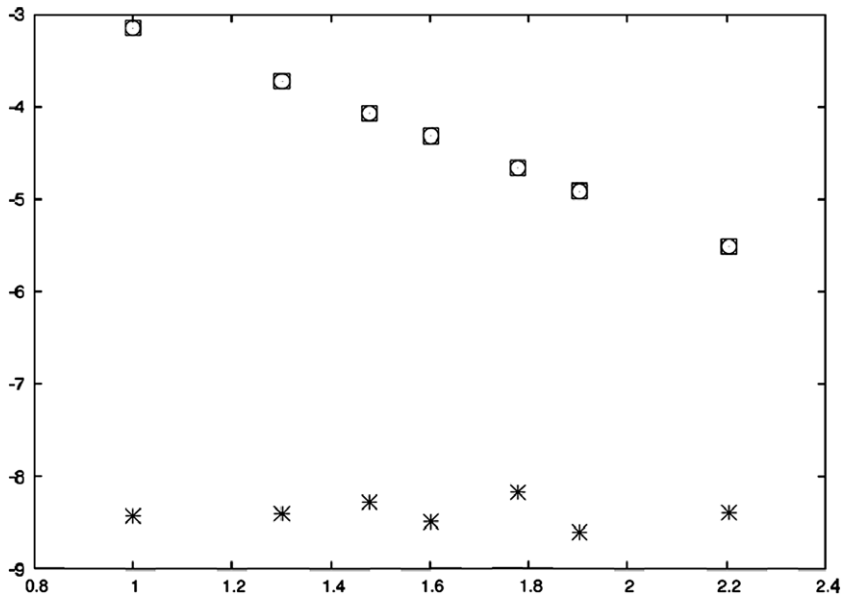


Fig. 5. Error,  $\Delta_W$ , defined in Eq. (58), as a function of lattice resolution,  $W$ , for our method of Section 3.1 for pressure driven flow in a uniform duct  $y = 0, W$  at constant  $Re = 0.5$ . LB collision parameter  $\tau = 3/2$  for this data. Values  $\tau = 1, 2$  produce no change in the data visible to the eye. The results in this figure comprise two almost overlying, sets of points (a) and (b). Data sets (a) and (b) are based upon different choices of the free variable  $f_i^{(0)}$ s – for the planar boundary of Section 3.1, set (a) corresponds to  $i = 0, 1, 2$ , set (b) to  $i = 0, 3, 4$ . In data set (a) open squares (diagonal crosses) represent unforced boundaries  $\phi_i = 0, y = 0, W$  (forced boundaries  $\phi_i \neq 0, y = 0, W$ ). In data set (b) open circles (erect crosses) represent unforced boundaries  $\phi_i = 0, y = 0, W$  (forced boundaries  $\phi_i \neq 0, y = 0, W$ ).

upon different choices of the free variable  $f_i^{(1)}$ s; in terms of the planar boundary  $y = W$  of Section 3.1, set (a) is characterised by choice  $i = 0, 1, 2$ , set (b) to choice  $i = 0, 3, 4$ . We return to this point below. In data set (a) open squares (diagonal crosses) represent unforced boundaries  $\phi_i = 0, y = 0, W$  (forced boundaries  $\phi_i \neq 0, y = 0, W$ ). In data set (b) open circles (erect crosses) represent unforced boundaries  $\phi_i = 0, y = 0, W$  (forced boundaries  $\phi_i \neq 0, y = 0, W$ ). In both sets (a) and (b), omitting the boundary force produces a linear variation in  $\log_{10} W$  with  $\log_{10} W$  of gradient  $\approx -2$ , characteristic of a spatially second-order accurate scheme; in the case of forced boundaries  $y = 0, W$ , the method of Section 3.1 appears to achieve a solution exact to machine precision, over the range of resolutions considered.

The fact that both data sets (a) and (b) in Fig. 5 correlate very well implies that our boundary closure method is insensitive to the choice of free variable  $f_i^{(1)}$ s. Our results also appear to show that the method is stable over a range of values of collision parameter  $2/3 < \tau < 2$ .

Fig. 6 shows corresponding reference data, obtained from two variants of bounce back boundary conditions. All data were obtained with collision parameter  $\tau = 1$ , corresponding to a known optimum of performance in the bounce-back method. In its defence, it should be noted that bounce back is adaptable, robust, versatile and easy to implement for both LBGK and LB methods, to generate *staircase* boundaries. That said, the limitations of the first-order accurate ‘on-link’ variant (open squares) are clear. Applying a boundary force to this method (open circles) apparently leaves the data unaffected. Mid-link bounce-back (diagonal crosses) approaches second order accuracy, almost certainly because its implementation here corresponds to drawing reflected  $f_i$ s from an ideally placed image of the channel with reversed flow (impossible in with a more complex geometry, note). For similar reasons, mid-link bounce-back with a boundary force (erect crosses) it achieves a small error, again approaching second order accuracy. None of the bounce-back methods recorded in Fig. 6 achieve the accuracy of the forced-boundary method of Section 3.1; neither can they be used to represent moving boundaries or boundaries. Discounting on-link bounce back, the data with the boundary forced has the smallest error. Symmetry arguments suggest that, with appropriate care, a forcing strategy for the mid-link bounce-back method *applied to the present geometry* might be devised, which promotes its accuracy to that of the current method. Clearly, this effort would have vary limited value.

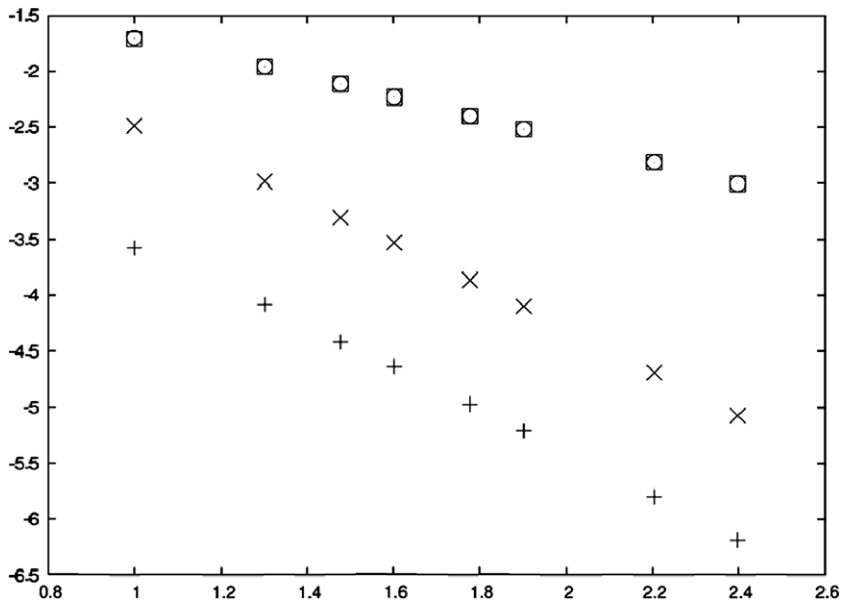


Fig. 6. Error,  $\Delta W$ , defined in Eq. (58), as a function of lattice resolution,  $W$ , for mid-link and nodal bounce-back boundary conditions. This data was obtained for pressure driven flow in a uniform duct  $y = 0, W$  with constant  $Re = 0.5$ . For all data in this figure, the collision parameter  $\tau = 1$ , corresponding to an optimum of performance for the bounce-back boundary method. Open squares (circles) correspond to nodal bounce-back (nodal bounce-back with a boundary body-force). Diagonal (erect) crosses correspond to mid-link bounce-back (mid-link bounce-back with a boundary body-force).

In order to demonstrate the ability of our method to handle both a boundary force and a boundary velocity, sheared, duct flow was simulated. Shear and a uniform pressure gradient were simultaneously applied to an incompressible fluid, again confined in a uniform channel of constant width  $W = 80$ , bounded by surfaces  $y = 0, 80$ . Flow was driven by (i) a uniform pressure gradient,  $G = 3g$ , and (ii) a constant motion of the  $y = W$  boundary, which moved at velocity  $u_0\hat{x}$ . Various values  $u_0$  and  $G$  consistent with a constant  $Re = 0.5$  were used. For such unidirectional flow it is possible to superpose solutions of the uni-directional (linearized) Navier–Stokes equations with appropriate boundary conditions. In LB (lattice) units, the exact axial velocity profile is

$$v_0(y) = \frac{G}{6\rho\nu}y(W - y) + \frac{u_0}{W}y. \quad (59)$$

Figs. 7 and 8 show the variation of such axial velocity profiles,  $v_0(y)$ , with distance,  $y$ . Fig. 7 shows simulation data obtained for collision parameter  $\tau = 1$  for  $u_0 = 1 \times 10^{-3}, 2 \times 10^{-3}, 3 \times 10^{-3}$ ; Fig. 8 shows simulation data for  $\tau = 2/3$  for  $u_0 = 6 \times 10^{-3}, 7 \times 10^{-3}, 9 \times 10^{-3}$ , where all velocities are in LB units. In all cases, any difference with the analytical result above, in Eq. (59) is too small to be visible in Figs. 7 and 8, the error,  $\Delta W$ , taking an average value of  $-7.8$ , a value consistent with that in shown Fig. 5.

To assess the internal corner boundary closure of Section 3.2 a square, 2D lid-driven cavity with boundaries  $y = 0, x = 0, W$  and a moving lid  $y = W$  was simulated. This lid is taken to move with velocity  $\mathbf{u}_0$ . Later we will set  $\mathbf{u}_0 = u_0\hat{e}_x$ . To obtain results which may be validated in an original way and to illustrate the adaptability of our method, we introduce at this point a model variant. It is possible to simulate at  $Re = 0$  by using an adapted D2Q9 LBGK scheme, after Ladd and Verberg, [21]. Following Ladd and Verberg, simplify the equilibrium distribution:

$$f_i^{(0)} = t_p\rho\left(1 + \frac{1}{c_s^2}\mathbf{v}\cdot\mathbf{c}_i\right), \quad (60)$$

producing a D2Q9 LBGK model otherwise identical to that considered in Sections 2 and 3.1. Analyzing with the particular Chapman–Enskog approach of Hou et al. in Ref. [19], it is possible to obtain a *steady-state* behaviour:

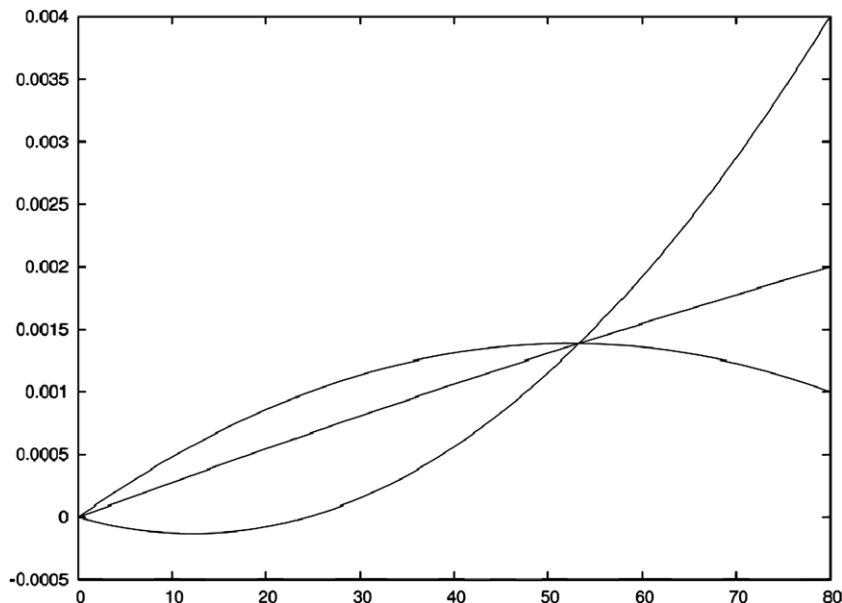


Fig. 7. Sheared, pressure driven flow velocity profiles obtained from simulations using our boundary closure of Section 3.1. For this data,  $Re = 0.5$ , collision parameter  $\tau = 1$  and the right-hand wall velocity  $u_0 = 1 \times 10^{-3}, 2 \times 10^{-3}, 3 \times 10^{-3}$ , where all velocities are in LB units.

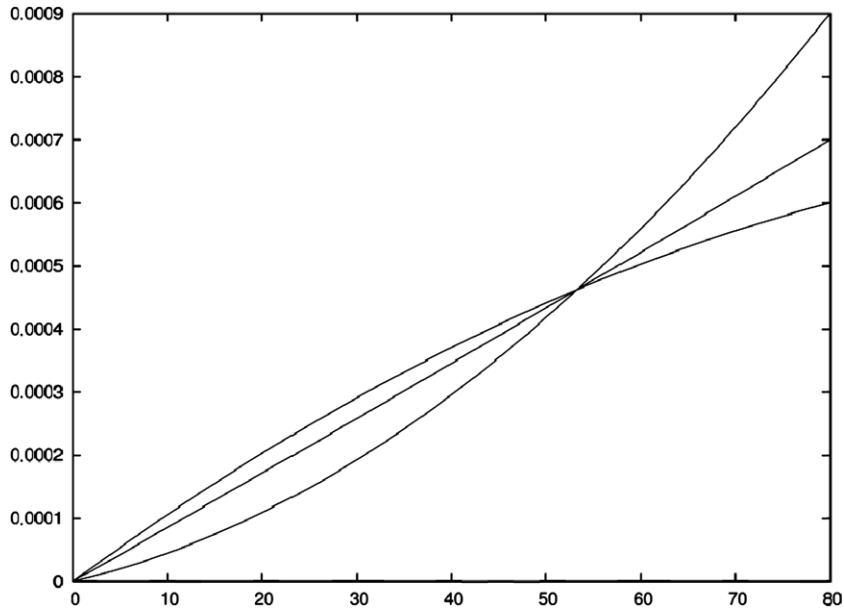


Fig. 8. Sheared, pressure driven velocity profiles obtained from simulations using our boundary closure of Section 3.1. For this data,  $Re = 0.5$ , collision parameter  $\tau = 2/3$  and the right-hand wall velocity  $u_0 = 6 \times 10^{-3}, 7 \times 10^{-3}, 9 \times 10^{-3}$ .

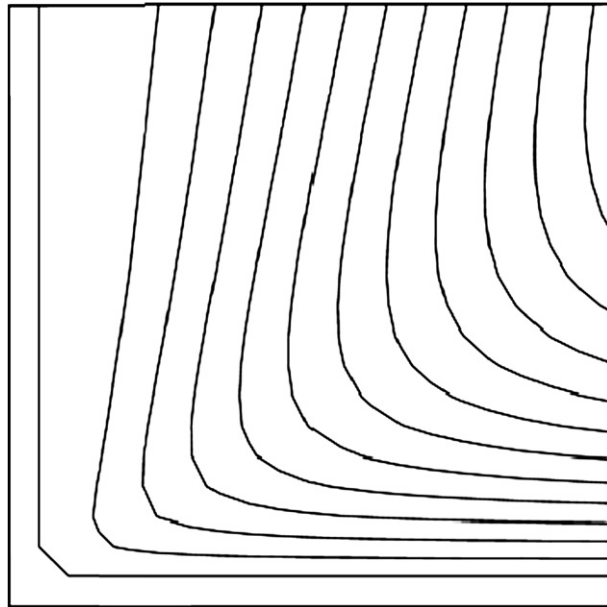


Fig. 9. Corner detail of the rectangular stream function contours of a steady-state, 2D, square lid-driven cavity. This data was obtained for  $Re = 0$  Stokes flow. The large system size of 150 lattice units and the small lid velocity underly the good correspondence with the analytical solution of corner flow, shown in Fig. 10.  $\psi = 0$  on  $x = 0, y = 0$ ; the maximum value of  $\psi$  corresponds to  $\psi = 1.05 \times 10^{-4}$ .

$$\frac{\partial}{\partial x_\beta} \rho v_\beta = 0, \quad \frac{1}{6}(2\tau - 1)\nabla^2 \rho v_\beta - \frac{1}{3} \frac{\partial}{\partial x_\beta} \rho = 0, \tag{61}$$

which, with replacement  $\mathbf{v} \rightarrow \rho \mathbf{v}$ , represents the Stokes equations with pressure  $P = 1/3\rho$  and shear viscosity  $\eta = 1/6(2\tau - 1)$ . The results of Section 3 may be modified for this revised model. For example, in Section 3.1, Eq. (33) for the density is modified for use with the truncated equilibrium in Eq. (60):

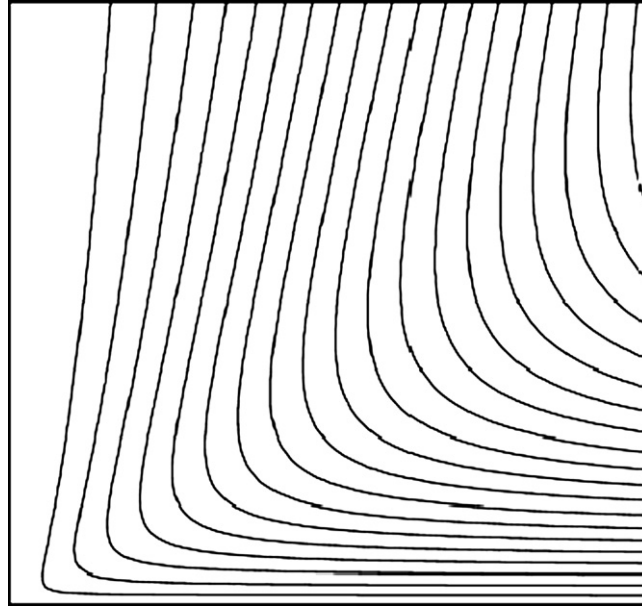


Fig. 10. Rectangular stream function,  $\psi$ , contours for two dimensional flow into a right-angled corner;  $130 < x < 150$ ,  $130 < y < 150$ ;  $\psi = 0$  on  $x = 0$ ,  $y = 0$ ; the maximum value of  $\psi$  corresponds to  $\psi = 9.5 \times 10^{-5}$ , in good agreement with the result in Fig. 9. Note the different contour interval in this image.

$$\rho' = \frac{M - \delta M}{\sum_{i \neq 1,2,3} t_p \left[ 1 + \frac{u_{0i} c_i}{c_s^2} \right]} = \frac{6M}{5 + 3u_{0y}}, \quad (62)$$

in which  $\delta M = 0$ , corresponding to no boundary force. Similar modifications must be made to the expressions for  $\rho'$  in the case of the internal corner, in Eq. (49):

$$\rho' = \frac{36(M - \delta M)}{25 + 24u_{0x} - 15u_{0y}}. \quad (63)$$

Using Eq. (60), the equilibrium,  $f_i^{(0)}$ , component of the boundary  $f_i$ s was assigned; boundary  $f_i^{(1)}$ s were calculated and the post-collision distribution assembled precisely after the method of Section 3.1.

Fig. 9 shows detail of the steady-state rectangular stream function, close to a corner of a rectangular, 2D, square lid-driven cavity. Here the stream functions should approximate the known solution of flow into a corner [26], which appears in Fig. 10, for reference. The large system size of 150 lattice units and the small lid velocity  $1.0 \times 10^{-4}$  underly encouraging correspondence with Fig. 10.

## 5. Conclusions

We have set-out and validated a very adaptable and accurate method for closing a lattice Boltzmann LBGK simulation lattice. Our method allows for both boundary motion and boundary fluid forces and its derivation demonstrates an accuracy consistent with the corresponding bulk scheme, it is instantaneously accurate and robust in that it functions with unimpaired accuracy for a range of values of LBGK collision parameters.

We have developed our boundary closure method for key flat and corner geometries; it may be applied to others. Overall we suggest that our method is as adaptable in this respect as popular bounce-back methods but, in addition, it has the added advantages of tractability, the capacity to handle both moving and stationary boundaries and the capacity to accommodate a fluid force at the boundary. The latter is of special significance to the wetting problem, to which we aim to apply our method.



## Appendix 1

In Section 3 a mass-conserving boundary closure algorithm was developed for a lattice fluid under a constant external force, like gravity. Here we detail the adjustments necessary in the analysis of Section 3 to account for variable external forces. Although simple and straightforward, these modifications strengthen the method considerably, opening-up a way correctly to include interfacial forces at the boundary.

Using the notation of Guo et al. [20] we will now show that, directly to generalize our analysis in Section 3 it is also necessary to re-interpret the fluid strain rate,  $S_{\alpha\beta}$ . We shall then state how the treatment of Section 3 should be modified to include variable external forces.

As previously stated, Guo et al. [20] showed that to recover Navier–Stokes behaviour in a lattice fluid subject to a variable external force,  $\mathbf{F}(\mathbf{r})$ , it is necessary to re-define the lattice fluid velocity of Eq. (9) [20]:

$$\rho \mathbf{v}^* = \sum_i f_i \mathbf{c}_i + \frac{1}{2} \mathbf{F}, \quad (64)$$

where  $\mathbf{v}^*$  is the fluid velocity. Note that it is  $\mathbf{v}^*$  which is assumed on the boundary, so, for example, a no-slip boundary would have  $\mathbf{v}^* = \mathbf{0}$ .

For the variable force LB model of Guo et al. equations (12) and (16) of Ref. [20] yield, after some straightforward algebra, an expression for the second moment of the  $f_i^{(1)}$ s which replaces that given in Eq. (16) of Section 3:

$$\sum_i f_i^{(1)} c_{i\alpha} c_{i\beta} = -\frac{\Delta t}{2} \left( v_\alpha^* F_\beta + v_\beta^* F_\alpha \right) - 2c_s^2 \tau \rho S_{\alpha\beta}^*, \quad (65)$$

where  $S_{\alpha\beta}^* = \frac{1}{2} \left( \frac{\partial v_\beta^*}{\partial x_\alpha} + \frac{\partial v_\alpha^*}{\partial x_\beta} \right)$  may be measured on the boundary.

Remembering that we have used  $\delta_i = 1$ , set  $\Delta t = \delta_i = 1$ , Eq. (65) may then be made to coincide with Eq. (16) by making the replacement:

$$S_{\alpha\beta} \rightarrow S_{\alpha\beta}^* + \frac{1}{4\tau\rho c_s^2} \left( v_\alpha^* F_\beta + v_\beta^* F_\alpha \right). \quad (66)$$

Recall, in our lattice closure method of Section 3, the boundary velocity and force are assumed to be known. Accordingly, all the terms in the right hand side of the map 66 may be evaluated. Therefore, simply by using the adjusted calculation of the measured boundary strain-rate, suggested by the map 66 above, our boundary closure method of Section 3 generalizes to the case of fluids under a variable external force.

## References

- [1] S. Succi, The lattice Boltzmann equation for fluid mechanics and beyond, Clarendon Press, 2001.
- [2] I. Halliday, L.A. Hammond, C.M. Care, A. Stevens, J. Phys. A: Math. Gen. 35 (2002) 157.
- [3] A.P. Hollis, I. Halliday, J. Phys. A: Math. Gen. 39 (2006) 10589.
- [4] A.W. Lees, S.F. Edwards, J. Phys. C 5 (1972) 1921.
- [5] A.J. Wagner, J.M. Yeomans, Phys. Rev. E 59 (1999) 4366.
- [7] A.J. Wagner, I. Pagonabarraga, J. Stat. Phys. 107 (2002) 521.
- [8] For a review, see e.g. S. Goldstein, The Mechanics of Fluids, Clarendon Press, Oxford, 1939.
- [9] M.A. Gallivan, D.R. Noble, J.G. Georgiadis, R.O. Buckius, Int. Numer. Meth. Fluids 25 (1997) 249.
- [10] D.R. Noble, S. Chen, J.G. Georgiadis, R.O. Buckius, Phys. Fluids 7 (1995) 203.
- [11] X.Y. He, Q. Zou, L.S. Luo, M. Dembo, J. Stat. Phys. 87 (1997) 115.
- [12] Q. Zou, X. He, Phys. Fluids 9 (1997) 1591.
- [13] S. Chen, D. Martinez, R. Mei, Phys. Fluids 8 (1996) 2527.
- [14] T. Inamuro, M. Yoshino, F. Ogino, Phys. Fluids 7 (1995) 2928.
- [15] I.C. Kim, KSME Int. J. 14 (2000) 84.
- [16] P.A. Skordos, Phys. Rev. E 48 (1993) 4823.
- [17] I. Ginzbourg, D. d’Humières, J. Stat. Phys. 84 (1996) 927.
- [18] Y.H. Qian, D. d’Humières, P. Lallemand, Europhys. Lett. 17 (1992) 479.
- [19] S. Hou, Q. Zou, S. Chen, G.D. Doolen, A.C. Cogley, J. Stat. Phys. 118 (1995) 329.
- [20] Z. Guo, C. Zheng, B. Shi, Phys. Rev. E 65 (2002) 046308.

- [21] A.J.C. Ladd, R. Verberg, *J. Stat. Phys.* 104 (2001) 1191.
- [22] I. Halliday, L.A. Hammond, C.M. Care, K. Good, A. Stevens, *Phys. Rev. E* 64 (2001) 011208.
- [26] G.K. Batchelor, *Introduction to Fluid Dynamics*, Cambridge University Press, 1973.